Journal of Materials Chemistry C

Electrochemical reduction of europium(III) using tetra-n-octyl diglycolamide functionalized ordered mesoporous carbon microelectrodes

Journal:	*Journal of Materials Chemistry C*
Manuscript ID	TC-ART-02-2020-000824.R1
Article Type:	Paper
Date Submitted by the Author:	06-Apr-2020
Complete List of Authors:	Bertelsen, Erin; Colorado School of Mines, Chemistry; Colorado School of Mines Antonio, Mark; Argonne National Laboratory, Chemical Sciences & Engineering Division Trewyn, Brian; Colorado School of Mines, Chemistry Kovach, Nolan; Colorado School of Mines, Chemistry Shafer, Jenifer ; Colorado School of Mines, Department of Chemistry and Geochemistry

SCHOLARONE™
Manuscripts

ARTICLE

Electrochemical reduction of europium(III) using tetra-*n*-octyl diglycolamide functionalized ordered mesoporous carbon microelectrodes

Received 00th January 20xx,
Accepted 00th January 20xx

DOI: 10.1039/x0xx00000x

Erin R. Bertelsen,[a] Nolan Kovach, [a] Brian G. Trewyn,[a,b] Mark R. Antonio[c] and Jenifer C. Shafer*[a,d]

This work investigates the one-electron reduction of Eu(III) to Eu(II) with ordered mesoporous carbon (OMC) in cavity microelectrode (CME) systems. OMC materials with and without tetra-*n*-octyl diglycolamide (TODGA) functionalization were subjected to voltammetric measurements and compared with commercial carbon black Vulcan® XC-72. The electrochemical reduction of solution Eu(III) with unfunctionalized OMC, XC-72, and TODGA-functionalized OMC—both within the electrode matrix and on the electrode surface—is reported. The complexation of Eu(III) by TODGA-functionalized OMC prior to electrode preparation incorporates Eu(III) as part of the bulk electrode matrix. Under these conditions, the high capacitance obscures the Eu(III)/Eu(II) redox couple. A signal emerges above the background (capacitive) currents when 2-octanol is added to the TODGA-functionalized OMC as a wetting agent. In contrast, surface Eu(III)-TODGA complexation, when Eu(III) contacts the electrode surface exclusively after electrode preparation, provides a strong response. The addition of 2-octanol to TODGA reduces the capacitance of the electrode and narrows the Eu(III)/Eu(II) redox peak widths. The desorption by reductive stripping of Eu(II) was demonstrated using a 2-octanol modified TODGA OMC CME, opening the possibility for selective separation of Eu from adjacent trivalent lanthanides.

Introduction

The one-electron reduction of Eu(III) to Eu(II) is a facile process in solution electrolytes. The readily accessible electrode potential, –0.55 V vs. Ag/AgCl, for the Eu(III)/Eu(II) couple[1] and the comparatively stable divalent oxidation state[2] are the basis of historical and contemporary strategies to separate Eu from the adjacent trivalent lanthanides (Sm, Gd) and from its actinide electronic analog, Am(III).[3-8] The trivalent lanthanides are arguably some of the most difficult elements to separate because of the small decrease in ionic radii across the 4*f*-period.[9] As such, the electroanalytical chemistry of Eu provides a convenient entry to effective separation processes. A profusion of basic and applied research has shown that both photons and electrons (from appropriate reagents and through the controlled polarization of an electrode surface) can be tuned for the selective and efficient reduction of Eu(III) in aqueous and nonaqueous solution electrolytes.[10-14]

With conventional fluid electrolytes, three methods are commonly used to separate Eu(II) from its trivalent neighbors: (1) selective precipitation (with sulfate); (2) liquid-solid extraction chromatography (EXC), and; (3) liquid-liquid extraction (LLE).[15] Despite the extensive practical exploitation of the Eu redox response in separation science, very little direct information is known about its electroanalytical chemistry in chemical separations systems of direct relevance to practical liquid-solid and liquid-liquid extraction. To address this gap in knowledge, we have probed the electrochemical properties of Eu using carbonaceous extraction chromatographic materials with and without TODGA (*N*,*N*,*N*',*N*'-tetra-*n*-octyl diglycolamide). This amidic, neutral solvating extractant is of contemporary significance in the ALSEP (Actinide-Lanthanide SEParation) concept for actinide-lanthanide separation because of its exceptionally high affinity for the trivalent lanthanides,[16] particularly Eu.

Since its synthesis in 2001 by Sasaki et al.,[17] TODGA has been extensively studied for 4*f*/5*f*-element separations in EXC, LLE, and supported liquid membrane (SLM) systems.[16, 18] In LLE extraction systems, TODGA is known to coordinate with the trivalent lanthanides in a 3 : 1 (TODGA : Ln) stoichiometry[19-22] following the equilibrium equation:

$$Ln^{3+}{}_{\mathrm{aq}} + 3NO_3^-{}_{\mathrm{aq}} + 3TODGA_{\mathrm{org}} \rightleftharpoons Ln(NO_3)_3TODGA_{3\,\mathrm{org}} \quad (1)$$

Further, it has been shown that TODGA is highly selective for the light lanthanides.[17] This selectivity is attributed to the Ln(III)–TODGA complex outer-coordination sphere, which contains the charge-neutralizing counter anions along with water molecules.[19, 23] TODGA does not demonstrate a high uptake of the divalent alkaline earth cations.[24, 25] In view of the fact that the ionic radii of Sr(II) and Eu(II) are essentially

[a] Department of Chemistry, Colorado School of Mines, Golden, CO 80401, USA. Email: jshafer@mines.edu
[b] Material Science Program, Colorado School of Mines, Golden, CO 80401, USA.
[c] Chemical Sciences & Engineering Division, Argonne National Laboratory, Lemont, IL 60439, USA.
[d] Nuclear Science and Engineering Program, Colorado School of Mines, Golden, CO 80401, USA.
† Electronic Supplementary Information (ESI) available. See DOI: 10.1039/x0xx00000x

equivalent (1.30 and 1.31 Å, respectively, for CN = IX),[26] and that their chemistry is astoundingly similar,[27] it is not unreasonable to imagine that TODGA would only poorly extract Eu(II) and desorb it from TODGA-loaded carbonaceous EXC materials consisting of ordered mesoporous carbon (OMC).

Like other neutral, solvating extractants, TODGA tends to form reverse micelles with hydrophilic cores and hydrophobic ends. The exposed octyl chains create a lipophilic environment and may be involved in extended intermolecular interactions.[28, 29] The addition of modifiers, such as 2-octanol, break up the TODGA reverse micelles and hydrogen-bonding networks.[28, 29] The 2-octanol acts as a wetting agent, decreasing the lipophilicity of the extractant and allowing for greater diffusion of analytes within the extractant.

Considerable attention has been given to OMC since its development by Ryoo et al. in 1999.[30] The graphitic nature of OMC, giving rise to its electrical conductivity,[31] has attracted research efforts for use in energy conversion and storage,[32-35] catalysts,[36-42] electrochemical sensors,[34, 43-48] and biosensors.[34, 49-52] The desirable electrochemical properties of OMC stem from its highly ordered pore structure—allowing for fast diffusion of the analyte—and its high surface area.[44, 53] Furthermore, hard-templated OMC enables improved analyte diffusion, with larger average mesopore diameters, than soft-templated OMC. The large electroactive surface area of OMC results in a high specific capacitance desirable for electrical double-layer capacitor applications.[35] OMC materials are also resistant to acidic and basic environments, making them ideal lanthanide adsorbents.[54]

Generally, there are two methods to employ OMC materials in electrochemical devices. The first method uses OMC as the bulk material for carbon paste electrodes (CPE), while the second method uses the OMC as a thin surface coating on a solid electrode to produce a mesoporous carbon-modified electrode.[44, 49] In the present study, OMC and Vulcan® XC-72 were used as bulk conducting powders in cavity microelectrode (CME) voltammetry studies of the one-electron reduction of Eu(III) to Eu(II). The prospect for the electrochemical separation of Eu from trivalent lanthanides by reductive stripping was also examined by physisorbing OMC with TODGA (and TODGA modified with 2-octanol) for use in the CME. Insights into the non-Faradaic responses of the OMCs, as well as the Faradaic responses associated with the Eu(III)/Eu(II) couple for the Eu-TODGA complexes on the OMC systems by use of CME voltammetry, are cast in context of general developments in the chemistry of Eu(II) for applications in synthesis, medicine, and energy sciences.[55, 56] In this vein, the redox properties of Eu complexes with prospective application as MRI ligands[57] and in systems of relevance to hydrothermal geochemistry[58] have been studied extensively.

Experimental

Reagents

The *l*-MSN (large pore mesoporous silica nanoparticle) template was prepared according to previously reported literature.[59] Vulcan XC-72 was obtained from Cabot specialty carbon blacks. The extractant used was *N,N,N′,N′*-tetra-*n*-octyl diglycolamide (TODGA, Marshallton Research Laboratories Incorporated). Sulfuric acid (98%) and optima grade nitric acid (69%) were obtained from Fisher Scientific. Sucrose, $Eu(NO_3)_3{\cdot}5H_2O$, $LiNO_3$, and 2-octanol were purchased from Sigma-Aldrich. All chemicals were used as received. Ultrapure (> 18.2 MΩ cm) deionized water was used for all aqueous solutions and carbon synthesis steps.

Instrumentation

Europium extractions were completed using an Eppendorf ThermoMixer C and Eppendorf Centrifuge 5702 RH. Small scale europium extractions employed a VWR vortex mixer and BD Clay Adams Compact II Centrifuge. The gross $^{152/154}$Eu(III) gamma activity was monitored using a Packard Cobra II NaI(Tl) solid scintillation auto-gamma counter. Voltammetry data were obtained using a BAS 100B/W electrochemical analyzer, BASi reference electrode (Ag/AgCl, BASi MR-2052), Pt rod (0.064" diam.) auxiliary electrode, and a Pt wire cavity microelectrode (previously prepared in-house as described elsewhere)[60] with a microcavity of approximately 100 µm i.d. × 30 µm.

Synthesis of OMC

Large-pore ordered mesoporous carbon (OMC) was synthesized as previously described using a hard-templating method.[59] In a ceramic crucible, 2 g of *l*-MSN (BET surface area: 337 $m^2\ g^{-1}$; BJH pore volume: 1.2 $cm^3\ g^{-1}$) was dry mixed with 1.2 g of sucrose followed by the addition of 5.0 mL of water. After hand stirring until aggregate-free, 200 µL of concentrated sulfuric acid was pipetted into the suspension and mixed for 5 min by hand. During this time, approximately 2.0 mL of water was added to resuspend any OMC aggregated on the crucible sidewalls. The crucible was then placed into an air convection oven at 100 °C for 6 hr followed by 160 °C for 6 hr to drive partial carbonization of the polymerized glucose framework. This process was then repeated three more times adding 0.89 g, 0.12 g, and 0.21 g of sucrose, respectively, to ensure complete casting of the carbon precursor within the silica template pores. After this, the sample was loaded into a quartz combustion boat and carbonized in a horizontal tube furnace. Under argon flow of 150 sccm, the sucrose-OMC powder was heated from ambient to 600 °C (ramp rate 6.5 °C min^{-1}), 600 to 900 °C (ramp rate 1 °C min^{-1}), and held static at 900 °C for 6 hr. After cooling, the sample was divided into two 50 mL plastic centrifuge tubes and etched with 35 mL of 10% hydrofluoric acid overnight. The suspensions were centrifuged at 3750 ×*g* for 10 min, decanted, and washed with 35 mL of water. Three more water washes were followed by an ethanol wash to ensure removal of any residual fluoride ions. After decanting the ethanol, the wetted OMC was dried overnight in an open-air oven at 80 °C.

TODGA and TODGA/2-octanol physisorption

Functionalized electrode materials were prepared by suspending approximately 250 mg of OMC in 2.0 mL of methanol in a 15 mL plastic centrifuge tube. The suspension was

This journal is © The Royal Society of Chemistry 20xx

Please do not adjust margins

disaggregated in an ultrasonic bath for 5 min prior to the next step. A solution containing 145.2 mg of TODGA and 19.7 mg of 2-octanol, or 69.6 mg of TODGA and 55.4 mg of 2-octanol in 1.0 mL of methanol was added to the OMC suspension. Samples with TODGA only were loaded in two rounds with 100 mg of TODGA in 1.0 mL methanol each. Drying in an open-air oven at 80 °C overnight furnished the OMC surface with the extractant and surface modifier.

OMC material characterization

Nitrogen sorption analysis was performed using a Micromeritics TriStar II Surface Area and Porosity instrument. Prior to each analysis, approximately 100.0 mg of OMC was loaded into a sample tube and degassed under nitrogen flow at 60 °C for 6 hr. The surface area was obtained from Brunauer-Emmett-Teller (BET) theory derived from the adsorption branch in the range of $0.05 < P/P_0 < 0.30$, while pore volume and pore-size distributions were computed from Barrett, Joyner and Helenda method from the desorption branch of the isotherms. Isotherm morphology was used to qualitatively affirm the porosity of the materials. The TGA experiments were run on a TA Instrument Q50 Thermogravimetric Analyzer with a ceramic sample pan and a constant nitrogen flow of 50 mL min^{-1}. Approximately 20 mg of sample was loaded into the pan and subjected to a constant heat rate of 10 °C min^{-1} from ambient to 800 °C. The loadings of 2-octanol and TODGA onto the OMC were determined by defining the regions of mass loss (30 °C < 2-octanol < 250 °C < TODGA < 440 °C).

Europium extraction by functionalized OMC

A 1 M HNO_3 concentration was chosen to facilitate sufficient Eu(III) extraction by TODGA. As a neutral, solvating ligand, TODGA extracts the trivalent lanthanides under moderate to high nitric acid conditions.[61] The acidic europium(III) nitrate solutions were prepared by dissolving $Eu(NO_3)_3{\cdot}5H_2O$ in 1 M HNO_3 so that the initial Eu(III) concentrations were 0.050 and 0.425 M. A 9 mL aliquot of the Eu(III) solution was then contacted with 90 mg of functionalized OMC material in a 15 mL centrifuge tube. Contacts were made at ambient temperature (23 °C) for 60 min followed by centrifugation at 3000 × *g* with the Eppendorf 5702 RH. The aqueous phase was removed using a fine tip plastic transfer pipet. The remaining damp Eu-loaded OMC material was transferred to folded weigh paper and sandwiched to remove excess aqueous solution. The OMC material was then left to dry in air before transferring to a microcentrifuge tube for storage.

The extraction process was also done on a small scale using 5 mg of functionalized OMC, 0.495 mL of Eu(III) solution, and 5 µL of an approximately 3.5 mM $^{152/154}$Eu(III) radiotracer in 0.001 M HNO_3 (prepared as previously described by Drader et al.).[62] After contacting, 350 µL aliquots of the supernatant aqueous phase was taken for gross gamma counting. The activity of the functionalized OMC was determined by delta calculation. These values were used to approximate the Eu(III) loading in the functionalized OMC electrode materials.

Cavity microelectrode preparation

A small mass of carbonaceous material was placed on a microscope slide. Any aggregated material was manually broken up between weigh paper using a glass stir rod. The cavity microelectrode was filled by firmly pressing the empty cavity against the carbonaceous material on the microscope slide. Filling of the cavity was confirmed using a magnifying glass prior to use. After use, the CME was cleaned by sonicating for 10 s in ethanol followed by sonication for 10 s in water. The CME was then dried in air before packing with new material.

Voltammetry

Differential pulse voltammetry (DPV) and cyclic voltammetry (CV) data were collected at room temperature (23 °C) in 1 M $LiNO_3$ (pH 6.7), unless otherwise stated. The DPV data were acquired at 20 mV s^{-1}. For three-phase-electrode voltammetry,[63-65] a 5 mL solution of 0.5 M TODGA in *n*-dodecane was contacted with an equal volume of a 0.6 M $Eu(NO_3)_3$–3 M $LiNO_3$ solution at ambient temperature, 21 ± 0.5 °C, according to standard techniques in LLE. The clear and colorless third phase in the usual location between the bottom, aqueous equilibrium phase and the upper, organic equilibrium phase was isolated for voltammetry.

Results and discussion

OMC material properties

The BET surface area and pore characteristics for the electrode materials are given in Table 1 (see ESI† Figure S1). The nitrogen physisorption isotherms reveal a high surface area (1241 $m^2\ g^{-1}$) for the OMC. Pore volume distributions gleaned from the desorption branch for OMC show a pore diameter *c.a.* 5 nm with a narrow distribution (ESI† Figure S1, inset). Further characterization, including TEM images and low angle XRD, are provided in the ESI† (Figures S2 and S3, respectively). As expected, with the addition of TODGA or TODGA/2-octanol the surface area and average pore width decrease.[59] The TGA results are shown in ESI† Figure S4. The repeated TODGA loading for the OMC sample without 2-octanol afforded the highest weight percent loading (34 wt% TODGA). The 2-octanol modified samples show deviations from the theoretical loadings of about 35 wt% TODGA/5 wt% 2-octanol and 19 wt% TODGA/15 wt% 2-octanol. TGA show the actual extractant loadings to be 22 wt% TODGA/4 wt% 2-octanol and 16 wt% TODGA/8 wt% 2-octanol, respectively.

Table 2. Amount of Eu(III) sorbed to OMC materials at equilibrium.

Material	Initial $[Eu(NO_3)_3]$, M	Sorbed Eu(III), mg g^{-1}
34 wt% TODGA OMC	0.050	28.6(7)
	0.425	460(10)
22 wt% TODGA/	0.050	16.6(4)
4 wt% 2-octanol OMC	0.425	670(20)
16 wt% TODGA/	0.050	37.1(9)
8 wt% 2-octanol OMC	0.425	530(10)

Europium extraction by functionalized OMC

Europium(III) extraction by 34 wt% TODGA OMC, 22 wt% TODGA/4 wt% 2-octanol OMC, and 16 wt% TODGA/8 wt% 2-octanol OMC was determined using a $^{152/154}$Eu(III) radiotracer following Equation 2:

$$q_e = \left(\frac{A_0 - A}{A_0}\right)\left(\frac{V}{m}\right) C_0 \qquad (2)$$

where q_e is moles Eu(III) sorbed per g of solid material at equilibrium, A_0 and A are the activities (cpm) of the aqueous phase before and after equilibrium, respectively, V is the volume (L) of the aqueous phase, m is the mass (g) of the solid material, and C_0 is the initial molar concentration of Eu(III) in the aqueous phase. Table 2 shows the initial Eu(III) concentrations and the approximate Eu(III) sorbed onto the functionalized OMC materials. All contacts were done once. Errors shown are ± 1σ determined from the counting statistics propagated through the calculation. The amount of sorbed Eu(III) found in the radiotracer studies was assumed to reflect the Eu(III) sorbed on the materials in the bulk extractions.

Carbonaceous CME capacitance

Capacitance measurements were made as a baseline characterization of the CME materials and demonstrate that no faradaic response occurs with the functionalization by TODGA or modification with 2-octanol. OMC materials are graphitic, mesoporous, and have a high surface area, making them suitable candidates in electrical double-layer capacitor applications.[56, 67] Pristine Vulcan XC-72 was used as a comparative conductive porous carbonaceous material for the unfunctionalized OMC. The capacitance of the materials was determined from CV data collected at scan rates of 9–100 mV s^{-1} in the polarization window of –1.0 to 0.0 V. The data for both materials exhibit a flat and featureless response with a rectangular shape (Figures 1a and b) indicative of a electrical double-layer capacitor,[68] albeit with distortion most prominent between –0.8 and –1.0 V. The capacitance was calculated using Equation 3:[69]

$$|I_a - I_c| = 2C(\mathrm{d}V/\mathrm{d}t) \qquad (3)$$

where I_a and I_c are the anodic and cathodic currents (A), respectively, C is the capacitance (F), and dV/dt is the scan rate (mV s^{-1}). The capacitive currents for the Vulcan XC-72 and unfunctionalized OMC were measured at –0.5 V.

Previous work by Zhou et al.[70] established that both surface area and porosity play a significant role in the capacitance of carbonaceous materials. Specifically, higher surface area increases capacitance but only if the surface area is accessible to the electrolyte ions. That is, the surface area created by *micro*pores is negated in its influence for capacitance; therefore, high *meso*porosity is desirable in the design of carbon-based electrical double-layer capacitors. The Vulcan XC-72 has a wide distribution of porosity, including micropores (< 2 nm), whereas the pore size distribution for the OMC is considerably narrower (ESI† Figure S1).[66] The high surface area and mesoporosity of the OMC material gives rise to its electrical double-layer capacitor properties as demonstrated by Figure 1b. The unfunctionalized OMC provides a geometric specific capacitance of 0.211 F cm^{-2} (using the geometric surface area of the microelectrode, 7.85 × 10^{-5} cm^2), nearly an order of magnitude greater than Vulcan XC-72 (0.0262 F cm^{-2}).

Table 1. BET surface area and pore characteristics for electrode materials.

	Vulcan XC-72[66]	OMC	34/0 OMC[a]	22/4 OMC[b]	16/8 OMC[c]
BET surface area (m^2 g^{-1})	237	1241	529	619	553
Average pore diameter (nm)	10.4[d]	4.7/5.0	4.3	4.0	4.1
Total pore volume (cm^3 g^{-1})	0.62	1.30	0.73	0.85	0.79

[a]34 wt% TODGA OMC, [b]22 wt% TODGA/4 wt% 2-octanol OMC, [c]16 wt% TODGA/8 wt% 2-octanol OMC. [d]The pore size distribution ranges from micro- (< 2 nm) to meso-porous (2–40 nm).[66]

The cyclic voltammograms in Figure 1c are for the 34 wt% TODGA functionalized OMC CME in 1 M $LiNO_3$. In the polarization window between –1.0 and 0.0 V, no redox events from TODGA are observed, and the response is flat and featureless. The CV wave shapes are less rectangular than the unfunctionalized OMC; nevertheless, the capacitance was evaluated at –0.6 V. The increasing slope, particularly of the anodic response, with increasing scan rate causes deviation from linearity in plots of the capacitive current (Figure 1c inset). The resulting capacitance is 7.0(3) µF with a geometric specific capacitance of 0.0892 F cm^{-2}.

The addition of 2-octanol as a wetting agent to the hydrophobic TODGA was examined using two different dilutions. The capacitive cyclic voltammograms for 22 wt% TODGA/4 wt% 2-octanol OMC and 16 wt% TODGA/8 wt% 2-octanol OMC CMEs are presented in Figures 1d and e, respectively. The capacitance of the electrode material decreased with increasing amounts of 2-octanol, with the 16 wt% TODGA/8 wt% 2-octanol OMC nearing the specific capacitance of Vulcan XC-72 at 0.0293 F cm^{-2}. Moreover, the wave shapes are less rectangular than the bare carbonaceous materials, indicating a deviation away from an electrical double-layer capacitor. With the addition of the modifier, 2-octanol, the data of Figure 1 demonstrate that the capacitance decreases. As the mesopores of the OMC are filled by the TODGA (or

Table 3. Slope regression coefficients of linear least squares fits for the I_{cap} versus scan rate, υ, for Vulcan XC-72 and unfunctionalized OMC (Figures 1a and b, respectively) along with the calculated absolute capacitance and geometric specific capacitance.

Material	Slope	R^2	Absolute C (µF)	Geometric specific C (F cm^{-2})
Vulcan XC-72	0.00411(3)	0.9995	2.05(2)	0.0262
OMC	0.0331(2)	0.9997	16.6(1)	0.211
34/0 OMC[a]	0.0140(7)	0.9805	7.0(3)	0.0892
22/4 OMC[b]	0.0133(7)	0.9964	6.6(1)	0.0841
16/8 OMC[c]	0.0047(2)	0.9851	2.3(1)	0.0293

[a]34 wt% TODGA OMC, [b]22 wt% TODGA/4 wt% 2-octanol OMC, [c]16 wt% TODGA/8 wt% 2-octanol OMC

This journal is © The Royal Society of Chemistry 20xx

Please do not adjust margins

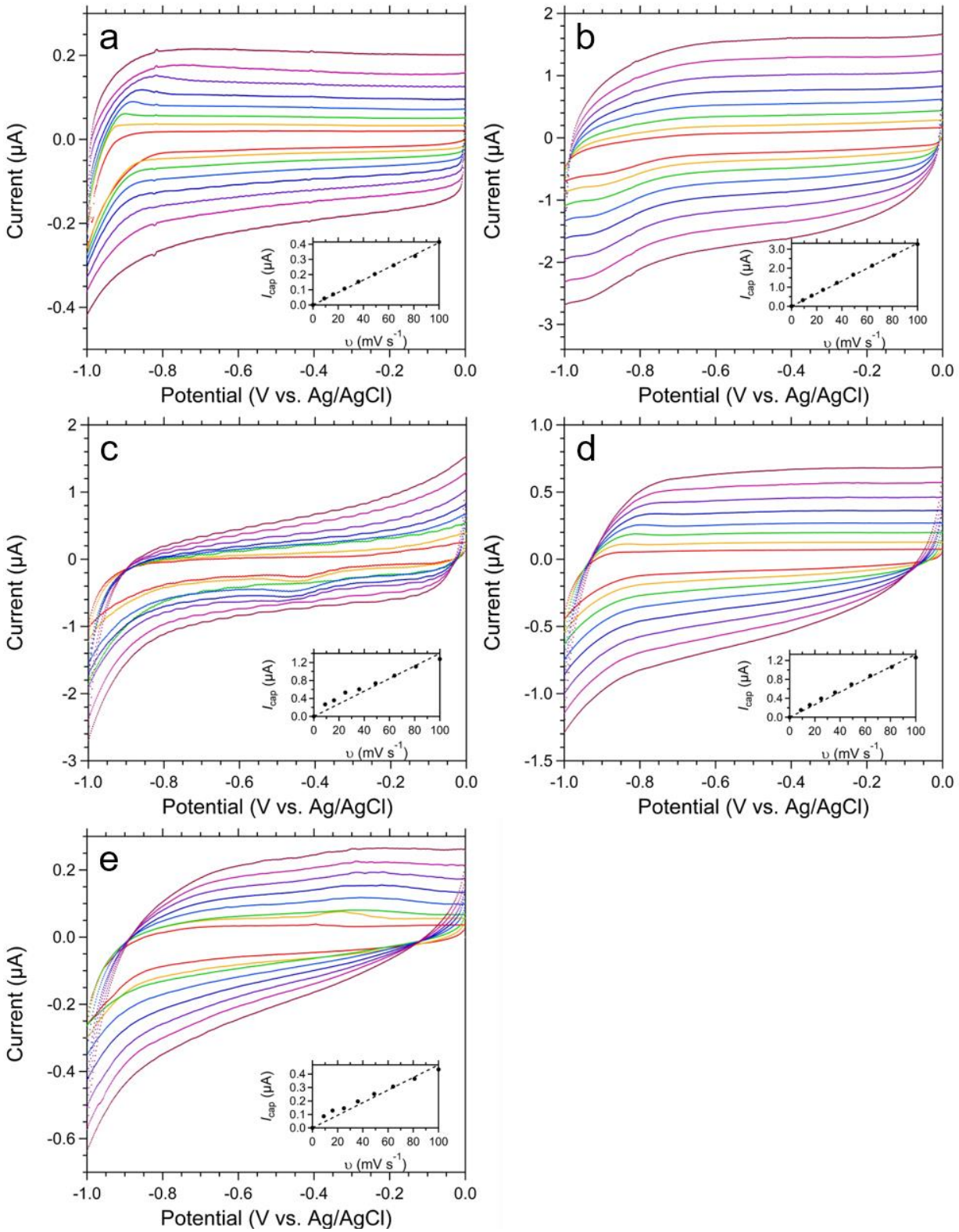

Figure 1. Capacitive cyclic voltammograms (a–e) and the corresponding capacitive current dependencies on scan rates (insets) using Vulcan XC-72 (a), unfunctionalized OMC (b), 34 wt% TODGA OMC (c), 22 wt% TODGA/4 wt% 2-octanol OMC (d), and 16 wt% TODGA/8 wt% 2-octanol OMC CMEs (e) in 1 M $LiNO_3$ electrolytes at scan rates of 9, 16, 25, 36, 49, 64, 81, and 100 mV s^{-1}. Capacitive currents were measured at –0.5 V on the unfunctionalized Vulcan XC-72, unfunctionalized OMC, 22 wt% TODGA/4 wt% 2-octanol OMC, and 16 wt% TODGA/8 wt% 2-octanol OMC CVs and at –0.6 V on the 34 wt% TODGA OMC CV.

TODGA and 2-octanol), the surface area decreases as does the capacitance. A summary of the absolute and geometric specific capacitances is given in Table 3.

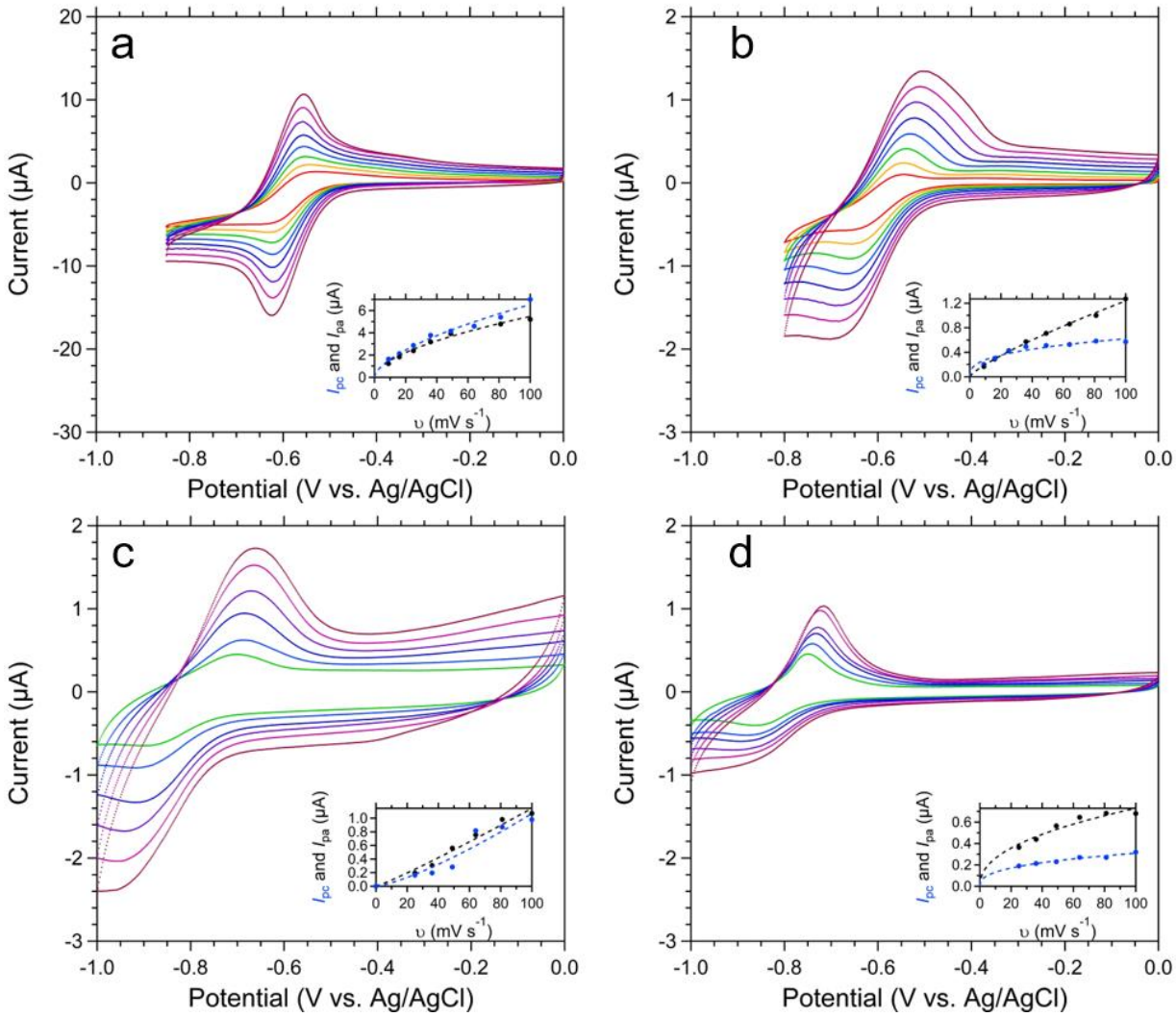

Figure 2. Faradaic cyclic voltammograms (a–d) and corresponding cathodic and anodic peak current intensities (I_{pc} and I_{pa}, respectively) as a function of scan rate (insets). CV data was obtained using unfunctionalized Vulcan XC-72 (a) and unfunctionalized OMC (b) CMEs in 0.100 M $Eu(NO_3)_3$/1 M $LiNO_3$ at scan rates of 9, 16, 25, 36, 49, 64, 81, and 100 mV s^{-1}. The 34 wt% TODGA OMC (c) and 16 wt% TODGA/8 wt% 2-octanol OMC (d) CMEs were contacted with 0.100 M $Eu(NO_3)_3$/1 M HNO_3 for 10 s prior to collecting CV data in 1 M $LiNO_3$ at scan rates of 25, 36, 49, 64, 81, and 100 mV s^{-1}. The negative cathodic peak current intensities were made positive for power law dependence evaluation, shown in Table 5.

Electrochemical behavior of the Eu(III)/Eu(II) redox couple using unfunctionalized carbonaceous CMEs

Cyclic voltammograms were recorded in a polarization window between –0.85 and 0.0 V for unfunctionalized Vulcan XC-72 and –0.8 and 0.0 V for unfunctionalized OMC CMEs in 0.100 M $Eu(NO_3)$/1 M $LiNO_3$ (Figure 2a and b) at scan rates of 9–100 mV s^{-1}. The cathodic and anodic peaks associated with the reduction and oxidation of Eu, respectively, are significantly narrower using the Vulcan XC-72 electrode than the OMC. Each peak was fit using a Gaussian and a cubic function baseline (capacitance) subtraction.[71] The fits were used to determine peak positions (E_p, V), peak currents (i_p, μA), and the peak width at half maximum ($W_{1/2}$, V). The half-wave potentials ($E_{1/2}$, V), peak separations (ΔE_p, V), and peak widths at half maximum presented in Table 4 are in line with the responses for the aquated Eu(III)/Eu(II) cations.[1, 2, 72] (Additional parameters are provided in ESI† Table S1.) Because the Eu(III)/Eu(II) redox peaks obtained with unfunctionalized OMC deviate from the ideal sigmoidal current-potential shape exhibited by Vulcan XC-72, the fits are a best approximation. Nonetheless, the voltammetric reductions of the aquated Eu(III) cation at Vulcan XC-72 and OMC working electrodes exhibit features that are typical of the electrochemically quasi-reversible process described by Botta et al.[73] Of particular note is the presence of isoamperic point potentials (at approx. –0.8 V and –0.1 V) in the data of Figure 2a–d that show where the faradaic reactions switch from oxidizing to reducing and vice versa.[74]

Information about the nature of the electron transfer process can be obtained from plots of peak currents with varying scan rates. For electrochemically reversible systems with freely diffusing redox species, this relationship is described according to Equation 4:[75]

$$i_p = 0.4463nFAC_O\left(\frac{nF\upsilon D_0}{RT}\right)^{1/2}. \qquad (4)$$

Here, n is the number of electrons per molecule transferred in the redox event, F is Faraday's constant, A is the electrode surface area (cm^2), C_0 is the bulk concentration of the oxidized species (mol L^{-1}), ν is the scan rate (mV s^{-1}), D_0 is the diffusion

This journal is © The Royal Society of Chemistry 20xx

Please do not adjust margins

coefficient of the oxidized species ($cm^2\ s^{-1}$), R is the universal gas constant, and T is absolute temperature. By comparison, for reversible systems with surface adsorbed species, the peak current response is defined by Equation 5:[75]

$$i_p = n^2F^2\upsilon A\Gamma^*(4RT)^{-1}. \quad (5)$$

Here, Γ^* is the surface coverage of the adsorbed species (mol cm^{-2}). By simplifying Equations 4 and 5, a general power law relationship (Equation 6) can be used to elucidate the electron transfer process.

$$i_p = a\upsilon^b \quad (6)$$

Table 4. Half-wave potentials ($E_{1/2}$)[a], peak separations (ΔE_p)[b], and peak widths at half maximum ($W_{1/2}$) for the observed Eu(III)/Eu(II) couples in the cyclic voltammograms from Figure 2 using unfunctionalized Vulcan XC-72 and OMC cavity microelectrodes as well as TODGA-functionalized OMC cavity microelectrodes.

υ (mV s^{-1})	$E_{1/2}$ (V)[a]	ΔE_p (V)[b]	$W_{1/2,c}$ (V)	$W_{1/2,a}$ (V)
		Vulcan XC-72		
9	–0.589	0.041	0.094	0.088
16	–0.589	0.035	0.090	0.091
25	–0.589	0.036	0.089	0.088
36	–0.590	0.039	0.090	0.088
49	–0.590	0.044	0.084	0.088
64	–0.590	0.049	0.080	0.081
81	–0.590	0.054	0.079	0.076
100	–0.590	0.064	0.083	0.073
avg.	–0.5896(5)	0.05(1)	0.086(5)	0.084(7)
		OMC		
9	–0.596	0.064	0.115	0.100
16	–0.594	0.071	0.117	0.108
25	–0.593	0.086	0.127	0.117
36	–0.590	0.100	0.133	0.130
49	–0.588	0.114	0.133	0.142
64	–0.585	0.121	0.133	0.159
81	–0.581	0.132	0.140	0.177
100	–0.580	0.143	0.136	0.205
avg.	–0.588(6)	0.10(3)	0.129(9)	0.14(4)
		34 wt% TODGA OMC		
25	–0.790	0.167	0.131	0.138
36	–0.787	0.185	0.136	0.156
49	–0.784	0.185	0.137	0.166
64	–0.794	0.231	0.195	0.174
81	–0.795	0.244	0.190	0.179
100	–0.795	0.250	0.200	0.180
avg.	–0.791(5)	0.21(4)	0.17(3)	0.17(2)
		16 wt% TODGA/8 wt% 2-octanol OMC		
25	–0.800	0.109	0.127	0.102
36	–0.800	0.121	0.137	0.098
49	–0.797	0.132	0.148	0.113
64	–0.796	0.135	0.163	0.122
81	–0.793	0.138	0.161	0.101
100	–0.792	0.145	0.179	0.098
avg.	–0.796(3)	0.13(1)	0.15(2)	0.11(1)

[a]$E_{1/2} = (E_{p,c} + E_{p,a})/2$, where $E_{p,c}$ and $E_{p,a}$ are the cathodic and anodic peak potentials, respectively. [b]$\Delta E_p = E_{p,a} - E_{p,c}$

Cathodic and anodic peak current intensities (I_{pc} and I_{pa}, respectively) taken from the CV waves in Figure 2a and b are plotted against scan rate for unfunctionalized Vulcan XC-72 and OMC and are shown in the corresponding insets. The scan rate exponential value, b, and the fitting parameter, a, are detailed in Table 5. The Vulcan XC-72 has a scan rate power law dependency near 0.5, indicating a reversible electrochemical electron transfer process of a freely diffusing Eu species (Equation 4). Conversely, the unfunctionalized OMC is better fit with opposing extremes, that is, $b > 0.5$ and $b < 0.5$ for the anodic and cathodic peak current intensities, respectively. The anodic peak, with $0.5 < b < 1$, suggests that both diffusion and surface adsorption electron transfer processes may be occurring. The irregularity of the cathodic peak current intensity exponent is attributed to the limitation of the Gaussian goodness of fit in the original peak fitting.

DPV data obtained with the unfunctionalized OMC CME as a function of Eu(III) analyte concentration show symmetrical responses that are equivalent to DPV data obtained with a conventional bulk working electrode, see ESI† Figure S5. The DPV data for the unfunctionalized OMC confirm the corresponding CV responses with the CME. Together, the CV and DPV data provide benchmarking knowledge about the Eu(III)/Eu(II) couple for the aquated cations for comparison with the corresponding redox behaviors of the Eu(III) complexes on TODGA-functionalized OMC.

Electrochemical behavior of the surface contacted Eu(III)/Eu(II) redox couple using functionalized OMC CMEs

Cyclic voltammetry. A 34 wt% TODGA OMC CME was contacted with a 0.100 M $Eu(NO_3)_3$/1 M HNO_3 aqueous solution for 10 s to allow for Eu-TODGA complexation. Because maximum Eu(III) uptake was not needed to produce a faradaic response, short contact times were used. Following contact, the electrode was carefully dried and introduced to a 1 M $LiNO_3$ electrolyte (without Eu) to collect CV data. Figure 2c shows a shift of the Eu(III)/Eu(II) redox couple—with an average $E_{1/2}$ of –0.790(5) V—to more negative potentials compared to the unfunctionalized OMC CME response (Figure 2b). The negative shift in $E_{1/2}$ using the 34 wt% TODGA OMC CME, compared to the unfunctionalized OMC CME, indicates stabilization of the native Eu(III) (see Table 6 and ESI† Table S1) by complexation

Table 5. Fitting parameter (a) and scan rate exponential (b) found using a power law fit of peak current intensities (I_{pa} and I_{pc}) versus scan rate (υ) for the Eu(III)/Eu(II) redox couple shown in Figure 2.

	I_{pa}			I_{pc}		
	χ^2	a	b	χ^2	a	b
Vulcan XC-72	0.3397	0.41(7)	0.56(4)	0.5749	0.39(8)	0.61(5)
OMC	4.395×10^{-3}	0.032(4)	0.79(3)	1.309×10^{-2}	0.12(3)	0.35(6)
34/0 OMC[a]	2.271×10^{-2}	0.007(4)	1.1(1)	8.648×10^{-2}	0.003(3)	1.3(3)
16/8 OMC[b]	7.570×10^{-3}	0.09(3)	0.44(7)	5.068×10^{-4}	0.06(1)	0.37(4)

[a]34 wt% TODGA OMC, [b]16 wt% TODGA/8 wt% 2-octanol OMC

Table 6. Half-wave potentials from DPV shown in Figure 4 using a three-phase GCE system contacted with Eu-TODGA-*n*-dodecane and a 34 wt% TODGA OMC CME.

System	Electrolyte	$E_{1/2}$ (V)
Third-phase from LLE	3 M $LiNO_3$	–0.689
34 wt% TODGA OMC	1 M $LiNO_3$	–0.782

with TODGA. Metal-ligand complexation, in general, stabilizes the higher oxidation state of metal ions, here Eu(III). For example, CV measurements of Eu macrocycles by Tóth et al.[72] reveal stabilization of Eu(III). This situation is manifest by the electrode potentials for the Eu(III)/Eu(II) couples of the macrocycle complexes (with ODDA, ODDM, DOTA, and DTPA)[‡] that are more negative than that for the simple aquated cation, much like what is observed here. That is, coordination does not stabilize Eu(II). The non-sigmoidal shapes of the redox peaks in Figure 2c makes quantitative analysis difficult, particularly for the cathodic peak. The anodic and cathodic peak currents were not linearly proportional to either the scan rate or the square root of the scan rate as demonstrated by the power law fit (Figure 2c inset) according to Equation 6.

Figure 2d shows the CV data acquired for the CME consisting of 16 wt% TODGA/8 wt% 2-octanol OMC contacted with 0.100 M $Eu(NO_3)_3$/1 M HNO_3. The addition of 2-octanol exhibits a striking difference in the CV wave shape, especially for the anodic peak, compared to the response (Figure 2c) without 2-octanol. Nonetheless, the average $E_{1/2}$ for the 2-octanol modified TODGA OMC is –0.796(3) V, very similar to the 34 wt% TODGA OMC (average $E_{1/2}$ = –0.790(5) V). The anodic peak for the 16 wt% TODGA/8 wt% 2-octanol OMC is about 0.060 V narrower than the 34 wt% TODGA OMC (see Table 4).

The non-ideal (i.e., non-Nernstian) faradaic behavior of the Eu(III)/Eu(II) couple with the OMC electrodes—both unfunctionalized and functionalized (Figure 2b-d)—may be due to insufficient diffusion of Eu ions within the OMC pores. The OMC material, and particularly the TODGA-functionalized OMC systems, are hydrophobic. This property will inhibit the diffusion of the aqueous electrolyte within the mesopores. Another contribution to the non-ideal behavior of the OMC systems is attributed to the packing of the material into the CME as the packing process may cause some physical blockage of the channels and disrupt uniform pore distribution. Even though the packing process produces fresh electrodes, there are inevitable variations that lead to subtly different CMEs each time one is made.

In Figure 3, the successive CV sweeps demonstrate decreasing faradaic currents using the 16 wt% TODGA/8 wt% 2-octanol OMC. This is consistent with reductive stripping of Eu(II). The fading of the faradaic current upon repeated cycling was observed for each of the TODGA-functionalized OMC CMEs. Because TODGA has a low affinity for divalent metal ions,[25] reductive desorption of Eu(II) is possible using TODGA functionalized OMC materials. As Eu(III), complexed with TODGA, is reduced to Eu(II), the binding affinity is too low to maintain Eu-TODGA coordination and the Eu(II) is desorbed from the functionalized electrode material. In this way, the selective electrochemical stripping of divalent Eu from TODGA-functionalized OMC materials contacted with an aqueous trivalent lanthanide solution is realized. Further experiments to confirm Eu(II) desorption, such as in-situ XANES or XPS, could be executed to further probe this chemistry.

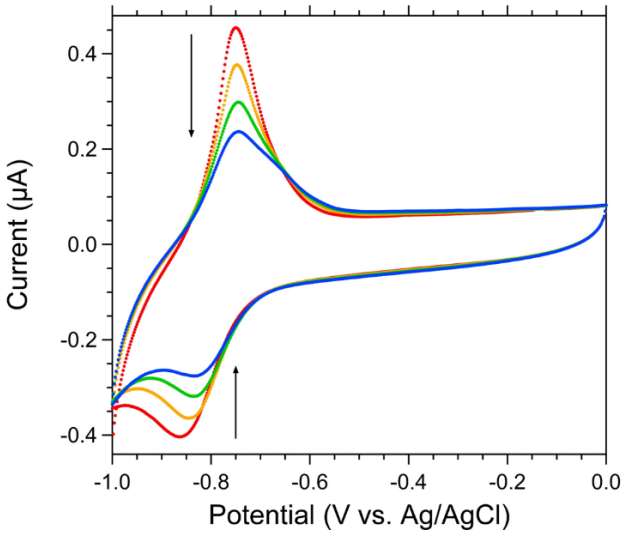

Figure 3. Cyclic voltammograms (obtained in a 1 M $LiNO_3$ electrolyte at 25 mV s^{-1}) for 16 wt% TODGA/8 wt% 2-octanol OMC after contact with 0.100 M $Eu(NO_3)_3$/1 M HNO_3. The first two segments are shown in red, followed by gold, green, and blue, successively.

Differential pulse voltammetry. The differential pulse voltammograms obtained for the three functionalized OMC electrodes (i.e., 34 wt% TODGA, 22 wt% TODGA/4 wt% 2-octanol, and 16 wt% TODGA/8 wt% 2-octanol after contact with 0.100 M $Eu(NO_3)_3$/1 M HNO_3) show comparable responses in terms of peak potentials, see Figure 4a. The signal strength and resolution of the Eu(III)/Eu(II) couple at approx. –0.80 V improves with increasing 2-octanol concentrations. Compared to the corresponding CV data of Figure 2, the better peak symmetry and shape afforded by DPV is due to the discrimination between the faradaic current and the background (capacitive) current, see Figure 1. The Eu electrode potentials obtained by use of CV and DPV are equivalent. To compare the response of these TODGA-functionalized-and-confined OMC electrodes with that for unconfined (i.e., solution phase) TODGA, three-phase electrode[65] DPV data was collected using a bulk GCE coated with an Eu-TODGA-*n*-dodecane third phase immersed in a 3 M $LiNO_3$ electrolyte. As shown in Figure 4b, the high concentration of the Eu-TODGA complex in the third phase provides a more intense Eu(III)/Eu(II) signal than for TODGA confined on the OMC. The shift of approx. –0.10 V in the half-wave potential (see Table 6) for the OMC system compared with the oil phase response demonstrates that Eu(III) is more stable in the confined environment with TODGA on the OMC than it is in the bulk oil phase from LLE. In other words, Eu(II) is more unstable on the TODGA-functionalized OMC than in the bulk oil. This is consistent with the reductive stripping observed in Figure 3.

This journal is © The Royal Society of Chemistry 20xx

Please do not adjust margins

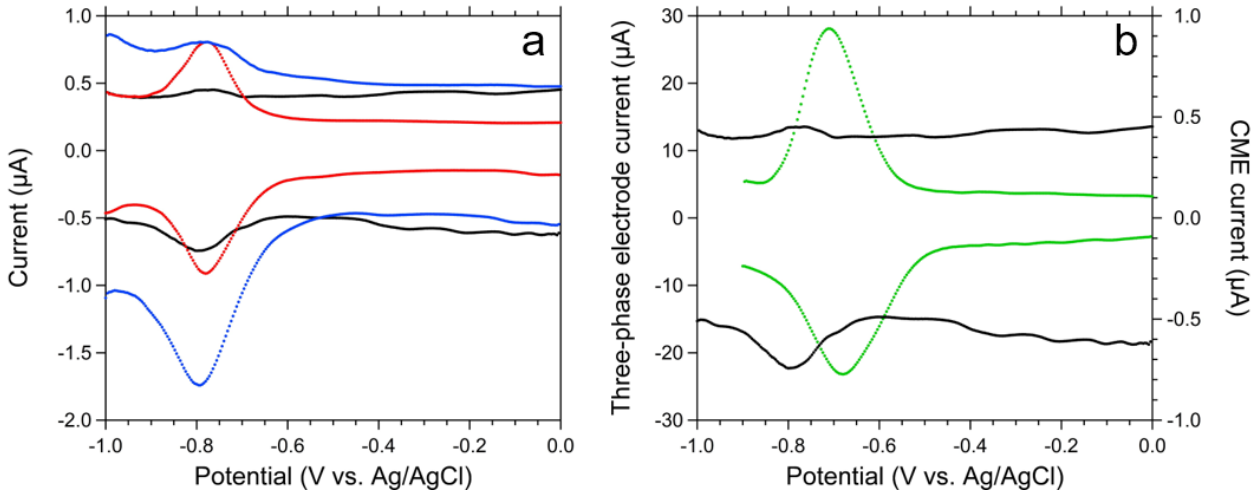

Figure 4. Differential pulse voltammograms obtained in 1 M $LiNO_3$ for (a, left) 34 wt% TODGA OMC (black, both panels), 22 wt% TODGA/4 wt% 2-octanol OMC (blue), and 16 wt% TODGA/8 wt% 2-octanol OMC (red) CMEs contacted with 0.100 M $Eu(NO_3)_3$/1 M HNO_3. (b, right) Three-phase electrode DPV for Eu-TODGA-n-dodecane third phase (green) obtained with a 3 M $LiNO_3$ aqueous electrolyte. The cathodic valleys (negative currents) were obtained in sweeps that began at the initial potential of 0 V, moving to decreasing electrode potentials. The anodic peaks (positive currents) were obtained in sweeps that began at the lowest electrode potential, moving to increasing ones.

The role of 2-octanol is one of a wetting agent, facilitating the diffusion of the analyte. The narrowing of Eu(III)/Eu(II) redox peaks with the addition of 2-octanol (cf. Figures 2c and 2d) is related to the system's electrochemical reversibility. That is, for an electrochemically reversible reaction, the peak width at half maximum (anodic or cathodic) in the DPV data will follow Equation 7:[75]

$$W_{1/2} = \frac{90.6}{n}\,\text{mV (25 °C)}. \qquad (7)$$

For the fully resolved anodic peak for the 16 wt% TODGA/8 wt% 2-octanol OMC CME, the width approaches the theoretical value of 90.6 mV for the one-electron oxidation of Eu(II) to Eu(III), see Table 7.

Electrochemical behavior of the matrix confined Eu(III)/Eu(II) redox couple using functionalized OMC CMEs

The complexation of Eu(III) by TODGA was accomplished by contacting the functionalized OMC with a $Eu(NO_3)_3$/1 M HNO_3 solution prior to OMC CME preparation to incorporate Eu(III) as part of the electrode matrix. The concentration of sorbed Eu(III) at equilibrium is presented in Table 2. DPV data were acquired for the three functionalized OMC electrodes (i.e., 34 wt% TODGA, 22 wt% TODGA/4 wt% 2-octanol, and 16 wt% TODGA/8 wt% 2-octanol) that were preloaded with different Eu(III) concentrations (e.g., 0.0–670 mg g^{-1}). In each of the systems examined, the Eu(III)/Eu(II) redox couples (ESI† Figure S6) are weak and poorly resolved by comparison with the response from the systems obtained through use of post-loading by surface contact alone, Figure 4a. The signal diminution and apparent passivation of the pre-loaded CMEs may be an artifact of the high capacitance of the material (obscuring the signal) or from the inability for electrolyte ions (e.g., Li^+, NO_3^-) to freely diffuse within the hydrophobic environment created by TODGA. Through the addition of 2-octanol as a wetting agent for TODGA, a stronger Eu(III)/Eu(II) redox couple appears. Again, multiple factors may be responsible as the addition of 2-octanol reduces the capacitance and acts as a surfactant—potentially aiding in ion mobility.

The DPV data shown in Figure 5 for the 22 wt% TODGA/4 wt% 2-octanol OMC system pre-loaded with 670 mg g^{-1} Eu(III) reveal additional complications. In particular, the cathodic peak potential was found to be sweep number dependent, moving to more negative electrode potentials after repeated sweeps, see Figure 5. For example, the initial cathodic peak (black curve) of the freshly prepared electrode resembles that for the aquated Eu cation ($E_{p,c}$ = –0.61 V). After electrode use, the cathodic peak

Table 7. DPV peak parameters from Figures 4, 5, and ESI† Figure S4 using unfunctionalized OMC.

		Cathodic peak			Anodic peak					
Electrode material	$[Eu(NO_3)_3]$, M[a]	E_p (V)	I_p (μA)	$W_{1/2}$ (V)	E_p (V)	I_p (μA)	$W_{1/2}$ (V)	$E_{1/2}$ (V)	ΔE_p (V)	$\lvert i_{pa}/i_{pc}\rvert$
OMC	0.0046	–0.583	–0.31	0.103	—	—	—	—	—	—
OMC	0.050	–0.581	–2.81	0.113	–0.606	0.95	0.110	–0.594	0.025	0.34
OMC	0.249	–0.584	–3.67	0.160	–0.598	2.13	0.149	–0.591	0.014	0.58
34/0 OMC[b]	0.100	–0.795	–0.18	0.117	–0.778	0.06	0.106	–0.780	0.018	0.34
22/4 OMC[c]	0.100	–0.788	–0.79	0.143	–0.771	0.16	0.137	–0.779	0.017	0.21
16/8 OMC[d]	0.100	–0.778	–0.45	0.107	–0.775	0.43	0.106	–0.777	0.003	0.95

[a]The unfunctionalized OMC had Eu(III) in electrolyte while functionalized OMC was contacted with Eu(III) prior to DPV data collection. [b]34 wt% TODGA OMC, [c]22 wt% TODGA/4 wt% 2-octanol OMC, [d]16 wt% TODGA/8 wt% 2-octanol OMC.

This journal is © The Royal Society of Chemistry 20xx

Please do not adjust margins

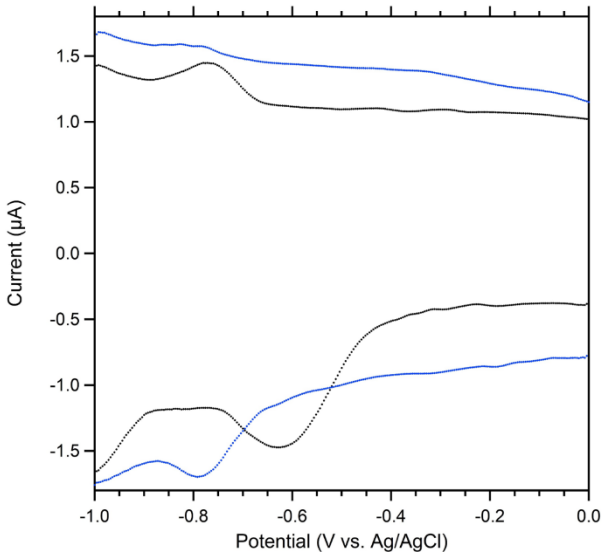

Figure 5. Differential pulse voltammograms using a 22 wt% TODGA/4 wt% 2-octanol OMC CME preloaded with 670 mg Eu(III) g^{-1} in 1 M $LiNO_3$. The black curve shows the initial response of a freshly prepared electrode. The blue curve shows the response after electrode use.

(blue curve) parallels that for complexed Eu-TODGA ($E_{p,c}$ = –0.78 V). Insight into this dependence is provided by data from batch sorption studies. In these, the highest Eu(III) loadings for each of the three materials is significantly greater than the stoichiometric limitations assumed through the complexation by TODGA given by Equation 1. The DPV data shown in Figure 5 suggests that Eu(III) in the TODGA OMC material at high metal loading is in a coordination environment different than the $Eu(NO_3)_3(TODGA)_3$ environment when less Eu(III) is loaded into the TODGA OMC. In these conditions, Eu is present in a hyper-stoichiometric amount relative to the TODGA, assuming a $Eu(NO_3)_3(TODGA)_3$ complex. As previous radiochemical analysis has demonstrated that unfunctionalized OMC does not participate in Eu(III) extraction,[59] the different coordination environment under high Eu(III) loading may be explained through admicelle formation. In admicelle formation, a fluid-like environment could be created within the admicelles that consists of condensed Eu(III)–$3NO_3$, water, and acid networks. Precedence for this scenario comes from LLE wherein high metal and/or acid extraction by TODGA in aliphatic diluents (without solvent modifiers, such as octanol) is prone to third phase formation and micelle formation.[16, 76, 77] In the initial, "fresh" scan, the Eu(III)/Eu(II) electrode potential approximates that of the hydrated cation and, perhaps, an admicelle like environment. After use, the excess Eu(III) is stripped from the fluid-like environment within the admicelles. The remaining Eu(III) is now presumably complexed as $Eu(NO_3)_3(TODGA)_3$ as the electrode potential is comparable to that observed in the voltammetry of the Eu(III)-TODGA-OMC material (see Figure 4a). Further consideration of this speciation is ongoing through the use of small-angle X-ray scattering experiments to examine the prospect of domain structures on OMC at the highest Eu loadings.

Conclusions

Cavity microelectrodes have been prepared with electrically conducting OMC powders loaded with the trivalent lanthanide-ion-selective extractant TODGA in combinations of 34 wt% TODGA OMC, 22 wt% TODGA/4 wt% 2-octanol OMC, and 16 wt% TODGA/8 wt% 2-octanol OMC. The TODGA functionalized OMC electrodes are capable of sorbing Eu(III) and through controlled polarization of the CME, the likely desorption of Eu(II) occurs. The unfunctionalized OMC electrodes exhibit electrical double-layer capacitor like CV shapes. This capacitance is reduced with TODGA functionalization, and further decreased with the addition of 2-octanol as an extractant modifier. The complexation of Eu by TODGA stabilizes the trivalent oxidation state, as evidenced by the half-wave potentials that are approx. 0.20 V more negative than that for the free aquated Eu cations. Moreover, the 2-octanol modifier appears to improve the ideality (i.e., reversibility) of the electrochemical process, an affect attributed to increasing the wettability of TODGA. Whereas OMC has better capacitive performance than Vulcan XC-72, the Vulcan CME provides a better voltammetric response than OMC for conventional (faradaic) solution studies of the Eu(III)/Eu(II) redox couple.

Conflicts of interest

There are no conflicts to declare.

Acknowledgements

The authors are grateful to Dr. Ke Yuan (Oak Ridge National Laboratory) for providing the cavity microelectrode used in the electrochemical studies. The Colorado School of Mines authors wish to acknowledge the funding provided by the Defense Threat Reduction Agency DTRA under grant number HDTRA1-16-0015). This work was also based upon support provided to E. R. Bertelsen by the U.S. Department of Energy, Office of Science Graduate Student Research (SCGSR) Program. M. R. Antonio acknowledges the support of the U. S. Department of Energy, Office of Science, Office of Basic Energy Sciences, Division of Chemical Sciences, Biosciences and Geosciences, under contract No DE-AC02-06CH11357.

Notes and references

‡ $DTPA^{5-}$ = diethylenetriamine-*N*,*N*,*N*',*N*'',*N*''-pentaacetate, $DOTA^{4-}$ = 1,4,7,10-tetraazacyclododecane-1,4,7,10-tertraacetate, $ODDM^{4-}$ = 1,4,10,13-tetraoxa-7,16-diazacyclooctadecane-7,16-dimalonate, and $ODDA^{2-}$ = 1,4,10,13-tetraoxa-7,16-diazacyclooctadecane-7,16-diacetate

Footnotes relating to the main text should appear here. These might include comments relevant to but not central to the matter under discussion, limited experimental and spectral data, and crystallographic data.

1 S. G. Bratsch, *Journal of Physical and Chemical Reference Data*, 1989, **18**, 1-21.

This journal is © The Royal Society of Chemistry 20xx

Please do not adjust margins

2 M. Van de Voorde, B. Geboes, T. Vander Hoogerstraete, K. Van Hecke, T. Cardinaels and K. Binnemans, *Dalton Transactions*, 2019, **48**, 14758-14768.
3 L. Jelinek, Y. Wei, T. Arai and M. Kumagai, *Solvent Extraction and Ion Exchange*, 2007, **25**, 503-513.
4 S. C. Li, S. C. Kim, C. S. Kang, C. J. Kim and C. J. Kang, *Hydrometallurgy*, 2018, **178**, 181-187.
5 D. F. Peppard, E. P. Horwitz and G. W. Mason, *Journal of Inorganic and Nuclear Chemistry*, 1962, **24**, 429-439.
6 J. S. Preston and A. C. du Preez, *Solvent Extraction and Ion Exchange*, 1991, **9**, 237-257.
7 J. S. Preston and A. C. du Preez, *Journal of Chemical Technology and Biotechnology*, 1996, **65**, 93-101.
8 M. Van de Voorde, K. Van Hecke, K. v. Binnemans and T. Cardinaels, *RSC Advances*, 2018, **8**, 20077-20086.
9 T. Moeller, in *The Chemistry of the Lanthanides*, ed. T. Moeller, 1973, DOI: 10.1016/B978-0-08-018878-2.50005-2, pp. 1-101.
10 A. G. Atanasyants and A. N. Seryogin, *Hydrometallurgy*, 1995, **37**, 367-374.
11 T. Donohue, *Optical Engineering*, 1979, **18**, 181-186.
12 T. Hirai and I. Komasawa, presented in part at the Solvent Extraction in the Process Industries, London, 1993.
13 J. M. Schwantes, R. Sudowe, H. Nitsche and D. C. Hoffman, *Journal of Radioanalytical and Nuclear Chemistry*, 2008, **276**, 543-548.
14 A. Yörükoğlu and İ. Girgin, *Hydrometallurgy*, 2002, **63**, 85-91.
15 A. Kumari, M. K. Jha, D. D. Pathak, S. Chakravarty and J.-c. Lee, *Separation & Purification Reviews*, 2019, **48**, 91-121.
16 S. A. Ansari, P. Pathak, P. K. Mohapatra and V. K. Manchanda, *Chemical Reviews*, 2012, **112**, 1751-1772.
17 Y. Sasaki, Y. Sugo, S. Suzuki and S. Tachimori, *Solvent Extraction and Ion Exchange*, 2001, **19**, 91-103.
18 D. Whittaker, A. Geist, G. Modolo, R. Taylor, M. Sarsfield and A. Wilden, *Solvent Extraction and Ion Exchange*, 2018, **36**, 223-256.
19 D. M. Brigham, A. S. Ivanov, B. A. Moyer, L. H. Delmau, V. S. Bryantsev and R. J. Ellis, *Journal of the American Chemical Society*, 2017, **139**, 17350-17358.
20 E. Metwally, A. S. Saleh and H. A. El-Naggar, *Journal of Nuclear and Radiochemical Sciences*, 2013, **13**, 1-7.
21 E. A. Mowafy and H. F. Aly, *Solvent Extraction and Ion Exchange*, 2007, **25**, 205-224.
22 Y. Sasaki, P. Rapold, M. Arisaka, M. Hirata, T. Kimura, C. Hill and G. Cote, *Solvent Extraction and Ion Exchange*, 2007, **25**, 187-204.
23 A. G. Baldwin, A. S. Ivanov, N. J. Williams, R. J. Ellis, B. A. Moyer, V. S. Bryantsev and J. C. Shafer, *ACS Central Science*, 2018, **4**, 739-747.
24 E. P. Horwitz, D. R. McAlister, A. H. Bond and R. Barrans Jr, *Solvent Extraction and Ion Exchange*, 2005, **23**, 319-344.
25 Y. Sasaki, Z. X. Zhu, Y. Sugo and T. Kimura, *Journal of Nuclear and Radiochemical Sciences*, 2007, **44**, 405-409.
26 R. D. Shannon, *Acta Crystallographica Section A*, 1976, **32**, 751-767.
27 S. Harder, *Angewandte Chemie International Edition*, 2004, **43**, 2714-2718.
28 S. Nave, G. Modolo, C. Madic and F. Testard, *Solvent Extraction and Ion Exchange*, 2004, **22**, 527-551.
29 P. N. Pathak, S. A. Ansari, S. Kumar, B. S. Tomar and V. K. Manchanda, *Journal of Colloid and Interface Science*, 2010, **342**, 114-118.
30 R. Ryoo, S. H. Joo and S. Jun, *The Journal of Physical Chemistry B*, 1999, **103**, 7743-7746.
31 A. Eftekhari and Z. Fan, *Materials Chemistry Frontiers*, 2017, **1**, 1001-1027.
32 J. Schuster, G. He, B. Mandlmeier, T. Yim, K. T. Lee, T. Bein and L. F. Nazar, *Angewandte Chemie International Edition*, 2012, **51**, 3591-3595.
33 C. Vix-Guterl, E. Frackowiak, K. Jurewicz, M. Friebe, J. Parmentier and F. Béguin, *Carbon*, 2005, **43**, 1293-1302.
34 A. Walcarius, *Chemical Society Reviews*, 2013, **42**, 4098-4140.
35 Y. Zhai, Y. Dou, D. Zhao, P. F. Fulvio, R. T. Mayes and S. Dai, *Advanced Materials*, 2011, **23**, 4828-4850.
36 J. Bai, X. Bo, D. Zhu, G. Wang and L. Guo, *Electrochimica Acta*, 2010, **56**, 657-662.
37 H. Chang, S. H. Joo and C. Pak, *Journal of Materials Chemistry*, 2007, **17**, 3078-3088.
38 J. K. Dombrovskis, H. Y. Jeong, K. Fossum, O. Terasaki and A. E. C. Palmqvist, *Chemistry of Materials*, 2013, **25**, 856-861.
39 M. Joglekar, S. Pylypenko, M. M. Otting, J. S. Valenstein and B. G. Trewyn, *Chemistry of Materials*, 2014, **26**, 2873-2882.
40 F. Li, K.-Y. Chan, H. Yung, C. Yang and S. W. Ting, *Physical Chemistry Chemical Physics*, 2013, **15**, 13570-13577.
41 A. K. Sahu, P. Sridhar and S. Pitchumani, *Journal of the Indian Institute of Science*, 2009, **89**, 437-445.
42 H. Wang, B. Qi, B. Lu, X. Bo and L. Guo, *Electrochimica Acta*, 2011, **56**, 3042-3048.
43 N. Jia, Z. Wang, G. Yang, H. Shen and L. Zhu, *Electrochemistry Communications*, 2007, **9**, 233-238.
44 A. Walcarius, *Trends in Analytical Chemistry*, 2012, **38**, 79-97.
45 A. Walcarius, *Electroanalysis*, 2015, **27**, 1303-1340.
46 J. Zang, C. X. Guo, F. Hu, L. Yu and C. M. Li, *Analytica Chimica Acta*, 2011, **683**, 187-191.
47 M. Zhou, J. Ding, L.-p. Guo and Q.-k. Shang, *Analytical Chemistry*, 2007, **79**, 5328-5335.
48 M. Zhou, L. Shang, B. Li, L. Huang and S. Dong, *Electrochemistry Communications*, 2008, **10**, 859-863.
49 A. Walcarius, S. D. Minteer, J. Wang, Y. Lin and A. Merkoçi, *Journal of Materials Chemistry B*, 2013, **1**, 4878-4908.
50 M. Zhou, L. Shang, B. Li, L. Huang and S. Dong, *Biosensors and Bioelectronics*, 2008, **24**, 442-447.
51 L. Zhu, C. Tian, D. Yang, X. Jiang and R. Yang, *Electroanalysis*, 2008, **20**, 2518-2525.
52 L. Zhu, C. Tian, D. Zhu and R. Yang, *Electroanalysis*, 2008, **20**, 1128-1134.
53 A. Walcarius, *Sensors*, 2017, **17**.
54 Z. Wang, A. T. Brown, K. Tan, Y. J. Chabal and K. J. Balkus, *Journal of the American Chemical Society*, 2018, **140**, 14735-14739.
55 L. A. Basal and M. J. Allen, *Frontiers in Chemistry*, 2018, **6**.
56 J. Garcia and M. J. Allen, *European Journal of Inorganic Chemistry*, 2012, **2012**, 4550-4563.
57 M. Gál, F. Kielar, R. Sokolová, Š. Ramešová and V. Kolivoška, *European Journal of Inorganic Chemistry*, 2013, **2013**, 3217-3223.
58 B. A. Bilal, *Zeitschrift für Naturforschung A*, 2014, **46**, 1108-1116.
59 E. R. Bertelsen, G. Deodhar, K. T. Kluherz, M. Davidson, M. L. Adams, B. G. Trewyn and J. C. Shafer, *Journal of Chromatography A*, 2019, **1595**, 248-256.
60 K. Yuan, D. Renock, R. C. Ewing and U. Becker, *Geochimica et Cosmochimica Acta*, 2015, **156**, 194-206.
61 Y. Sasaki, Y. Sugo, S. Suzuki and S. Tachimori, *Solvent Extraction and Ion Exchange*, 2001, **19**, 91-103.
62 J. A. Drader, L. Zhu, P. Smith, K. McCann, S. Boyes and J. C. Braley, *Separation and Purification Technology*, 2016, **163**, 352-356.
63 M. K. Bera, T. H. Bray, R. J. Ellis and M. R. Antonio, *ChemElectroChem*, 2014, **1**, 1173-1181.
64 R. J. Ellis, M. K. Bera, B. Reinhart and M. R. Antonio, *Physical Chemistry Chemical Physics*, 2016, **18**, 31254-31259.
65 F. Scholz and R. Gulaboski, *ChemPhysChem*, 2005, **6**, 16-28.

66 A. D. Moore, S. M. Holmes and E. P. L. Roberts, *RSC Advances*, 2012, **2**, 1669-1674.
67 P. Simon and Y. Gogotsi, *Nature Materials*, 2008, **7**, 845-854.
68 R. Lin, P. L. Taberna, J. Chmiola, D. Guay, Y. Gogotsi and P. Simon, *Journal of The Electrochemical Society*, 2009, **156**, A7-A12.
69 C. Portet, J. Chmiola, Y. Gogotsi, S. Park and K. Lian, *Electrochimica Acta*, 2008, **53**, 7675-7680.
70 S.-y. Zhou, X.-h. Li, Z.-x. Wang, H.-j. Guo and W.-j. Peng, *Transactions of Nonferrous Metals Society of China*, 2007, **17**, 1328-1333.
71 using Igor Pro 6 software from WaveMetrics, Inc.
72 É. Tóth, L. Burai and A. E. Merbach, *Coordination Chemistry Reviews*, 2001, **216-217**, 363-382.
73 M. Botta, M. Ravera, A. Barge, M. Bottaro and D. Osella, *Dalton Transactions*, 2003, DOI: 10.1039/B211533F, 1628-1633.
74 B.-Y. Chang, *Journal of Electrochemical Science and Technology*, 2017, **8**, 244-249.
75 A. J. Bard and L. R. Faulkner, *Electrochemical Methods: Fundamentals and Applications*, Wiley, 2 edn., 2000.
76 S. Tachimori, Y. Sasaki and S.-i. Suzuki, *Solvent Extraction and Ion Exchange*, 2002, **20**, 687-699.
77 D. Woodhead, F. McLachlan, R. Taylor, U. Müllich, A. Geist, A. Wilden and G. Modolo, *Solvent Extraction and Ion Exchange*, 2019, **37**, 173-190.

This journal is © The Royal Society of Chemistry 20xx

Please do not adjust margins

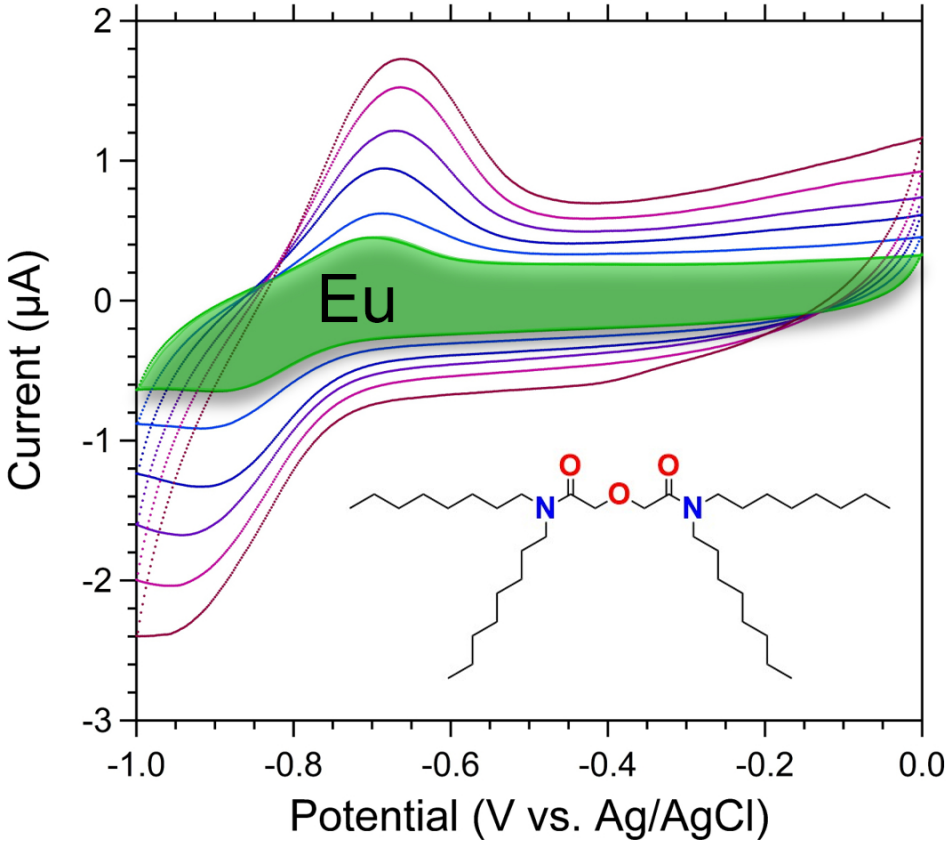
Eu
Current (μA)
Potential (V vs. Ag/AgCl)
2
1
0
-1
-2
-3
-1.0
-0.8
-0.6
-0.4
-0.2
0.0
O
O
O
N
N